Energies **2012**, *5*, 4147-4164; doi:10.3390/en5104147

OPEN ACCESS

energies

ISSN 1996-1073

www.mdpi.com/journal/energies

Article

Synthesis of Alcohols and Alkanes from CO and H_2 over MoS_2/γ-Al_2O_3 Catalyst in a Packed Bed with Continuous Flow

Sheng-Wei Chiang [1], Chia-Chi Chang [1], Je-Lueng Shie [2], Ching-Yuan Chang [1,3,*], Dar-Ren Ji [1], Jyi-Yeong Tseng [1], Chiung-Fen Chang [4] and Yi-Hung Chen [5]

1 Graduate Institute of Environmental Engineering, National Taiwan University, 71, Chou-Shan Road, Taipei 106, Taiwan; E-Mails: d96541003@ntu.edu.tw (S.-W.C.); d92541005@ntu.edu.tw (C.-C.C.); jdr0826@gmail.com (D.-R.J.); a9441187@gmail.com (J.-Y.T.)

2 Department of Environmental Engineering, National I-Lan University, I-Lan 260, Taiwan; E-Mail: jlshie@niu.edu.tw

3 Department of Chemical Engineering, National Taiwan University, 1, Section 4, Roosevelt Road, Taipei 106, Taiwan

4 Department of Environmental Science and Engineering, Tunghai University, Taichung 407, Taiwan; E-Mail: cfchang@thu.edu.tw

5 Department of Chemical Engineering and Biotechnology, National Taipei University of Technology, Taipei 106, Taiwan; E-Mail: yhchen1@ntut.edu.tw

***** Author to whom correspondence should be addressed; E-Mail: cychang3@ntu.edu.tw; Tel.: +882-223-638-994; Fax: +886-223-638-994.

Received: 25 August 2012; in revised form: 4 October 2012 / Accepted: 11 October 2012 / Published: 22 October 2012

Abstract: Effects of reaction conditions on the production of alcohols (AOHs) and alkanes (Alk) from CO and H_2, which can be obtained from the gasification of biomass, using a molybdenum sulfide (MoS_2)-based catalyst of MoS_2/γ-Al_2O_3 were studied. A high-pressure fixed packed bed (HPFPB) was employed to carry out the reaction. The results indicate that the conversion of CO (X_{CO}) and specific production rates of alcohol (SPR_{AOH}) and alkane (SPR_{Alk}) are highly depended on temperature (T). In T = 423–573 K, maximum yield of alcohols (Y_{AOH}) and SPR_{AOH} occur at T = 523 K. In the meantime, well performance gives the selectivity of ethanol (S_{EtOH}) of 52.0 C%. For the studies on varying H_2/CO mole ratio ($M_{H/C}$) from 1 to 4 at 523 K, the appropriate $M_{H/C}$ to produce EtOH is 2, giving higher ratios of SPR_{AOH}/SPR_{Alk} and Y_{AOH}/Y_{Alk} than those with other $M_{H/C}$. As for varying the total gas flow rates (Q_G) of 300, 450, 600 to 900 $cm^3\ min^{-1}$ tested at T = 523 K and $M_{H/C}$ = 2, the lower Q_G provides longer reaction time (or gaseous retention time, t_R) thus

offering higher X_{CO}, however lower productivity. For setting pressure (P_{ST}) = 225–540 psi, a supply of higher pressure is equivalent to providing a larger amount of reactants into the reaction system, this thus suggests the use of higher P_{ST} should give both higher X_{CO} and productivity. The assessment of the above results indicates that the MoS_2/γ-Al_2O_3 catalyst favors the production of alcohols over alkanes, especially for ethanol. The information obtained is useful for the proper utilization of biomass derived gases of CO and H_2.

Keywords: hydrogenation of CO; syngas; alcohol synthesis; alkanes synthesis; molybdenum sulfide

1. Introduction

The energy crisis has been an issue of great concern in recent years. With the continued climbing crude oil price, utilization of alternative energy has become more and more essential. The use of biomass, such as agriculture residues and woody waste, to provide energy and chemicals is receiving increasing interest because these resources can supplement the existing supplies of raw energy materials while have less net environmental impact [1–6]. Thus, bio-energy has the potential to provide a significant share of the projected renewable energy requirement in the future. As an example, ethanol (EtOH) has been broadly utilized as a good additive for enhancing the gasoline octane value and burning efficiency [1,7].

In the hydrogenation of synthesis gas (syngas), previous studies have shown that ethanol can be produced from syngas over many metal-containing catalysts, broadly classified into four categories. These include Rh-based catalysts [8], modified high-temperature and low-temperature methanol synthesis catalysts based on ZnO/Cr_2O_3 and $Cu/ZnO/Al_2O_3$ [9], respectively, modified Fischer-Tropsch catalysts based on Co, Fe and Ru [10], and non-sulfide [11] and sulfide Mo-based catalysts [12–14]. Among these catalysts, molybdenum sulfide (MoS_2) catalysts have attracted much interest because of their higher selectivity to alcohols and excellent resistance to poisoning from sulfur in the feed gas [15–19]. Previous studies also examined the effects of support on the Mo-based catalyst, indicating that the microstructures of MoS_2 clusters on Al_2O_3 supports strongly affect the interaction between Mo oxide and alumina. The interaction is related to the high dispersion of Mo oxide, which leads to highly active structures [16,18].

In previous studies [2], various reaction conditions were also tested for the applications of different catalysts in order to demonstrate the feasibility for the hydrogenation of CO. Inoue *et al*. [20] studied the applicability of Rh catalyst reporting the activation energy result and indicating that the selectivity of methane increases at higher temperatures. Hu *et al*. [21] in a study concerning Rh catalyst described the mechanism of methane formation and pointed out that the reaction is very sensitive to temperature. Thus, the formation of methane becomes dominant at higher temperatures.

Besides the temperature factor, the H_2/CO feed ratio is also a key adjustable variable affecting the conversion of syngas to ethanol or higher alcohols. Mazzocchia *et al.* [22] and Egbebi and Spivey [23] examined the effect of increasing H_2/CO ratio ($M_{H/C}$) on the formation of both EtOH and methane, showing that the selectivity for ethanol on Rh-based catalysts actually increases with increasing H_2/CO

ratio. Moreover, the H_2/CO can be adjusted to maximize S_{EtOH} and restrain methane formation. It is noted that methane is also a thermodynamically favorable product. However, its economical value is less than alcohols. The major formation reactions of ethanol and methane are as follows:

$$2CO_{(g)} + 4H_{2(g)} \rightarrow C_2H_5OH_{(g)} + H_2O_{(g)} \quad (1)$$

$\Delta H^0_{298} = -253.6$ kJ mol^{-1} and $\Delta G^0_{298} = -221.1$ kJ mol^{-1} of ethanol.

$$CO_{(g)} + 2H_{2(g)} \rightarrow CH_3OH_{(g)} \quad (2)$$

$\Delta H^0_{298} = -90.5$ kJ mol^{-1} and $\Delta G^0_{298} = -25.1$ kJ mol^{-1} of methanol.

$$CH_3OH_{(g)} + CO_{(g)} + 2H_{2(g)} \rightarrow C_2H_5OH_{(g)} + H_2O_{(g)} \quad (3)$$

$\Delta H^0_{298} = -165.1$ kJ mol^{-1} and $\Delta G^0_{298} = -97.0$ kJ mol^{-1} of ethanol.

$$CH_3OH_{(g)} + CO_{(g)} \rightarrow CH_3COOH_{(g)} \quad (4)$$

$\Delta H^0_{298} = -123.3$ kJ mol^{-1} and $\Delta G^0_{298} = -77.0$ kJ mol^{-1} of CH_3COOH.

$$CH_3COOH_{(g)} + H_{2(g)} \rightarrow C_2H_5OH_{(g)} \quad (5)$$

$\Delta H^0_{298} = -41.7$ kJ mol^{-1} and $\Delta G^0_{298} = -221.1$ kJ mol^{-1} of ethanol.

$$CO_{(g)} + 3H_{2(g)} \rightarrow CH_{4(g)} + H_2O_{(g)} \quad (6)$$

$\Delta H^0_{298} = -205.9$ kJ mol^{-1} and $\Delta G^0_{298} = -141.9$ kJ mol^{-1} of methane.

The competition of the above reactions and other side reactions of hydrogenation of CO thus greatly affects the selectivities of products by the heats and free energies of the associated reactions.

Hu *et al.* [21] also reported the roles of gas hourly space velocity (GHSV) as well as temperature, revealing that a lower GHSV results in higher EtOH, while a lower temperature gives less methane. As for the effect of system pressure, Spivey and Egbebi [1] indicated that an increasing pressure increases the equilibrium concentration of EtOH from the hydrogenation of CO following Le Chatelier's Principle.

In the hydrogenation of CO, molybdenum-based catalysts which have been also commonly used in the hydrogenation of petroleum have attracted much attention, especially alkali-modified catalysts. However, reports on the effects of operation conditions on the system performance employing MoS_2/γ-Al_2O_3 catalyst, which can be easily made, have been scarce. Thus, in this study, the hydrogenation of CO over MoS_2/γ-Al_2O_3 catalysts was practiced under various system conditions and examined concerning the production of alcohols and other hydrocarbons (HCs). The proper conditions to produce more alcohols, especially EtOH, with less methane were emphasized. Comparisons with the results using other catalyst were made to assess the corresponding effectiveness of hydrogenation of CO over various catalysts.

2. Experimental

2.1. Preparation of Catalysts

Mo-based catalysts were prepared employing the wet impregnation method. The catalyst support is γ-Al_2O_3 pellets (55.5 Å average pore diameter, 4 mm spherical pellet, 4–12 mesh), supplied by BDH Chemicals Ltd. (Poole, UK). It possesses a Brunauer-Emmett-Teller (BET) surface area of 280.46 m^2 g^{-1}. The γ-Al_2O_3 support was pre-calcined in air at 900 ℃ to avoid any structural changes during the

following high-temperature calcination for the preparation of catalyst. About 50 g dried γ-Al_2O_3 was impregnated with 100 mL of 5 wt.% aqueous solution of ammonium heptamolybdate [$(NH_4)_6Mo_7O_{24}{\cdot}4H_2O$], supplied by J.T. Baker (Phillipsburg, NJ, USA). The pH of the solution was controlled at 2.0 by adding nitric acid so as to avoid the overloading of the molybdenum. After being dried at 105 ℃ for 24 h, the sample was calcined at 500 ℃ for 6 h. The catalyst at this stage was denoted as Mo_XO_Y/γ-Al_2O_3. The resulted Mo_XO_Y/γ-Al_2O_3 was further reduced and sulfurized in the mixed gas stream of H_2S/H_2 with volume ratio of 5/95 at 673 K for 2 h to produce MoS_2/γ-Al_2O_3 catalyst. The molybdenum content in the final sample is about 34 mg g^{-1}. The above preparation procedures of catalyst are common, and the method is widely used because of its effectiveness.

2.2. Characterization of Catalysts

X-ray powder diffraction (XRD) patterns of the tested catalysts were obtained on a Rigaku TTRAX III powder diffractometer (Sendagaya, Shibuya-Ku, Tokyo, Japan) installing with the X-ray source of 18 kW rotating anode Cu target operated at wave length of 1.5456 Å, current of 20 mA and two theta from 20.020 to 110.000 deg using 4.0 deg min^{-1} of scanning speed. Scanning electron microscopy (SEM) images were carried out using JEOL JSM-7600F field emission scanning electron microscope (Akishima, Tokyo, Japan). The specific surface area (S_{BET}) was estimated by the BET equation using the data measured employing Micromeritics ASAP2020—physisorption analyzer (Norcross, GA, USA). The pore radius distribution and the mesopore analyses were obtained from the adsorption branch of the isotherm using the Barrett-Joyner-Halenda (BJH) method. The bulk particle density (ρ_P) and true density (ρ_S) (He displacement method) of catalysts were measured using Micromeritics AccuPyc II 1340 Pycnometer (Norcross, GA, USA).

2.3. Hydrogenation of CO

The experimental high-pressure fixed packed bed (HPFPB) system was set up as shown in Figure 1. CO and H_2 with purities of 0.9995 and 0.9995 were supplied by Ching-Fong Co. (Taipei, Taiwan). The syngas was provided from CO and H_2 cylinders with the mole ratio adjusted by mass flow controllers (MFCs) (Brooks 5850E Series, Hatfield, Philadelphia, PA, USA). Concentration of gas mixture was measured at pre-sampling port after the pre-mix chamber while before the HPFPB to confirm the steady inlet concentration. A 3/8 inch single-tube reactor packed with catalysts and spherical glass beads was vertically set and used in this study. For the pressure control, a regulator was installed for maintaining the system pressure and adjusting the output flow rate. The polar organic products such as alcohols and acids were collected by the absorption along with condensation using de-ionized (DI) water (4 ℃) in a condenser. Fresh catalyst and DI water were used for each run. Before the outlet gas from the packed bed flowed into the condenser, the gas was by passed and the instantaneous concentrations were measured at different subsequent times to ensure achieving the steady state. After reaching the steady state in the packed bed reactor, the gas was then introduced into the condenser. The unabsorbed and uncondensed gas was also examined for checking the steady state. Moreover, at the steady state, the cumulative concentrations of liquid samples measured over a period of time increased linearly with time, further assuring achieving the steady state. The linear slope can be used to obtain

the steady production rate (PR) of liquid product. Data at the steady state were thus used to compute the information needed.

Figure 1. Schematic diagram of apparatus for the hydrogenation of CO.

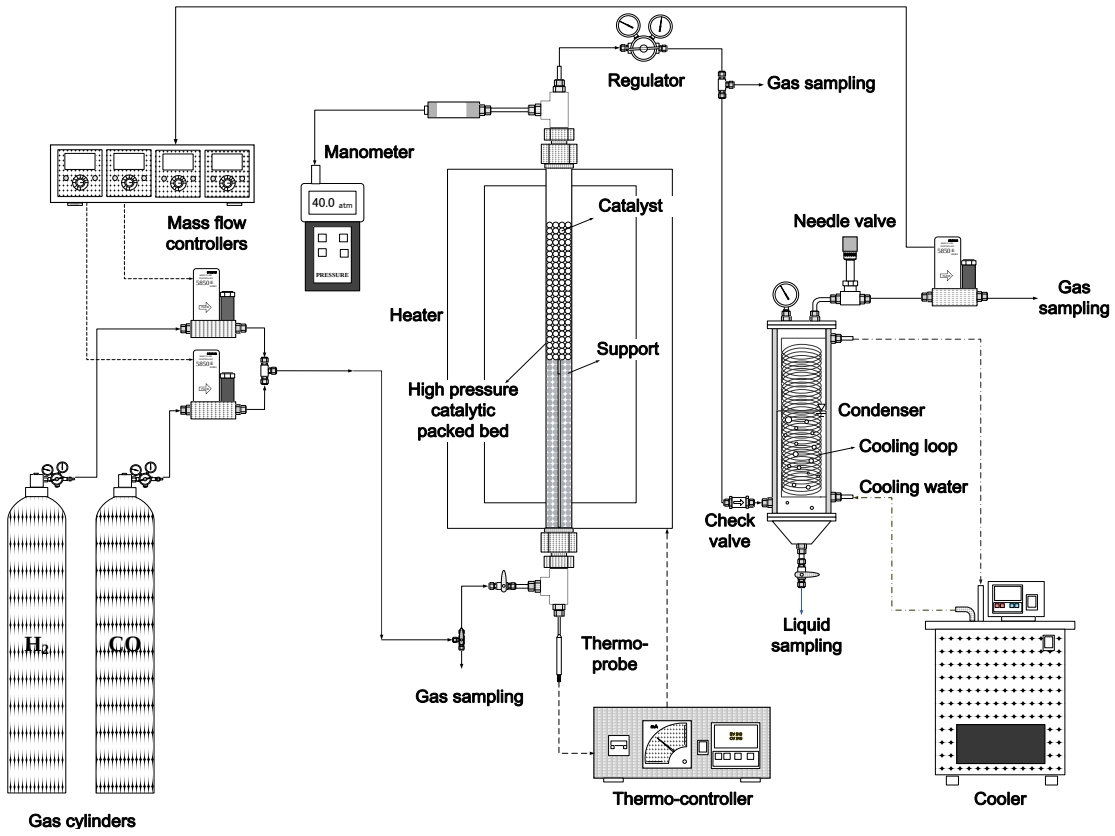

The HPFPB system was operated under the conditions with the H_2/CO mole ratio = 1–4, total gas flow rate of syngas (Q_G) = 300–900 cm^3 min^{-1}, temperature (T) = 423–573 K, mass of catalyst (m_S) = 25 g, and setting pressure (P_{ST}) = 225–540 psi (reading at 298 K). The base conditions were as follows unless otherwise specified: H_2/CO ratio $M_{H/C}$ = 2, mass flow rates of H_2 and CO (dm_{H2}/dt and dm_{CO}/dt) of 1.07 and 7.50 g h^{-1}, P_{ST} = 450 psi (30.6 atm) (reading at 298 K), m_S = 25 g, Q_G = 300 cm^3 min^{-1} and gas hourly space velocity GHSV = 1020 h^{-1}.

The conversion of CO is computed according to the following equation:

$$X_{CO}\,(\%) = (\Sigma\, N_j\, M_j/M_{CO,f}) = 1 - (M_{CO,p}/M_{CO,f}) \quad (7)$$

where N_j = number of carbon atoms in carbon-containing product j; M_j = mole of carbon-containing product j other than CO; $M_{CO,f}$ = mole of carbon monoxide in feed; $M_{CO,p}$ = mole of carbon monoxide in product stream.

The selectivity of product j is based on the total number of carbon atoms in the products and it therefore defined as:

$$S_j\,(\%) = N_j\, M_j/(\Sigma\, N_j\, M_j) \quad (8)$$

The yield of product j is also based on the total number of carbon atoms in the products and is defined as:

$$Y_j\,(\%) = N_j\, M_j/M_{CO,f} \quad (9)$$

2.4. Analyses of Liquid and Gaseous Samples

The analysis of gaseous organic compounds was performed using gas chromatography/flame ionization detector (GC/FID, 6890 GC, Agilent Technologies, Santa Clara, CA, USA) with an AB-5 column (30 m × 0.53 mm × 5.00 μm, Abel Industries, Pitt Meadows, BC, Canada). A purge-and-trap sample concentrator (Model 4560, OI Analytical, College Station, TX, USA) was used to purify and inject the liquid samples into GC/FID for analysis. For the calibration of GC/FID, the standards of C_1-C_4 alcohols (99.9%) and C_1-C_6 alkanes (99.9%) employed were obtained from Accustandard Inc. (New Haven, CT, USA) and Sigma-Aldrich Inc. (Shanghai, China), respectively.

The gaseous products of CO, CO_2 and H_2 were analyzed by two separate chromatography/thermal conductivity detector analyzers (GC/TCD, 8900 GC, China Chromatography Co., Taipei, Taiwan). The GCs are installed with the same packed columns (60/80 Carbonxen-1000, 15 ft × 1/8 in SS, Sigma-Aldrich, Saint Louis, MO, USA). Different carrier gases of helium (He) for the analyses of CO and CO_2 and argon (Ar) for that of H_2 were respectively used. For the calibration of GC/TCD, the standards of CO and CO_2 (99.995%) and H_2 (99.995%) used were supplied by Ching-Fong Co. Standard errors (σ_{n-1}) of data were computed to indicate the level of precision. For example, the σ_{n-1} of X_{CO} and PR_{HC} are about 2.6% and 4.3%.

3. Results and Discussion

3.1. Properties and Characteristics of Catalysts

The XRD patterns of MoS_2/γ-Al_2O_3 samples are shown in Figure 2.

Figure 2. The XRD patterns of MoS_2/γ-Al_2O_3 catalyst.

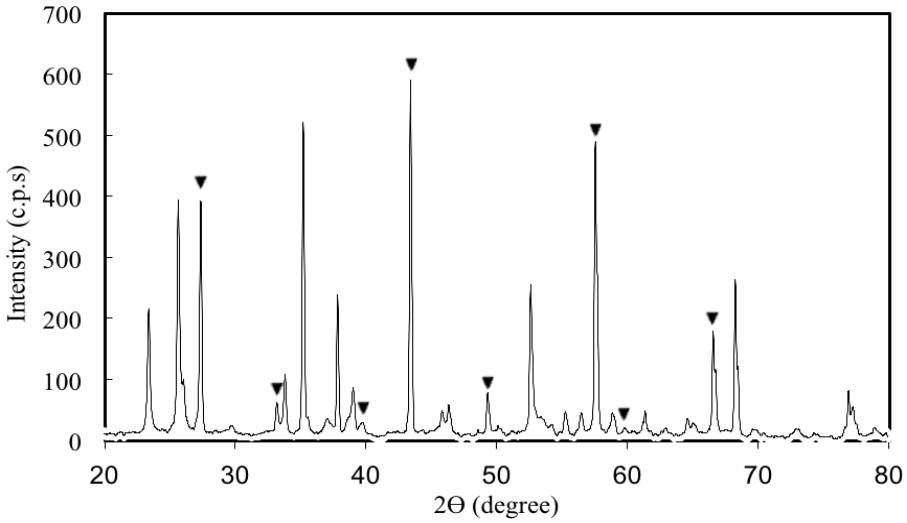

The peaks denoted with solid triangles (▼) at 2θ = 32.85°, 39.85°, 49.66°, 58.57°, 60.05° and 66.67 ° match the polygonal structure of MoS_2 (JCPDS No. 17-0744) in accordance with the characteristic peaks reported by Berdinsky *et al.* [24]. However, they also additionally noted 2θ at 28.86 ° and 43.99 ° for the MoS_2 nano-powder examined [24]. The SEM micrograph of sample in Figure 3a (magnification = 200×) indicates crystalline part of MoS_2 (noted by white ○), and

non-crystalline part of MoS_2 and surface of γ-Al_2O_3 (denoted by white Δ). The enlargement of Δ with magnification of 5000× is displayed in Figure 3b. The crystalline part of MoS_2 consists of polygonal particles which may exhibit lamellar structure as also noted by Ye *et al.* [25]. However, small clusters appear on the surface as shown in Figure 3b. The MoS_2 crystallite size estimated using Figure 3a is about 128 μm × 128 μm × 24 μm. More accurate size may be calculated by using Scherrer formula from XRD diffraction information. Moreover, further examination of the morphology properties using selected area electron diffraction in transmission electron microscopy may provide more clear identification of the structures of crystalline and non-crystalline MoS_2.

Figure 3. SEM micrographs of MoS_2/γ-Al_2O_3 catalysts: (**a**) crystalline of MoS_2 (○) and non-crystalline part of MoS_2 and surface of γ-Al_2O_3 (Δ); (**b**) enlargement of Δ.

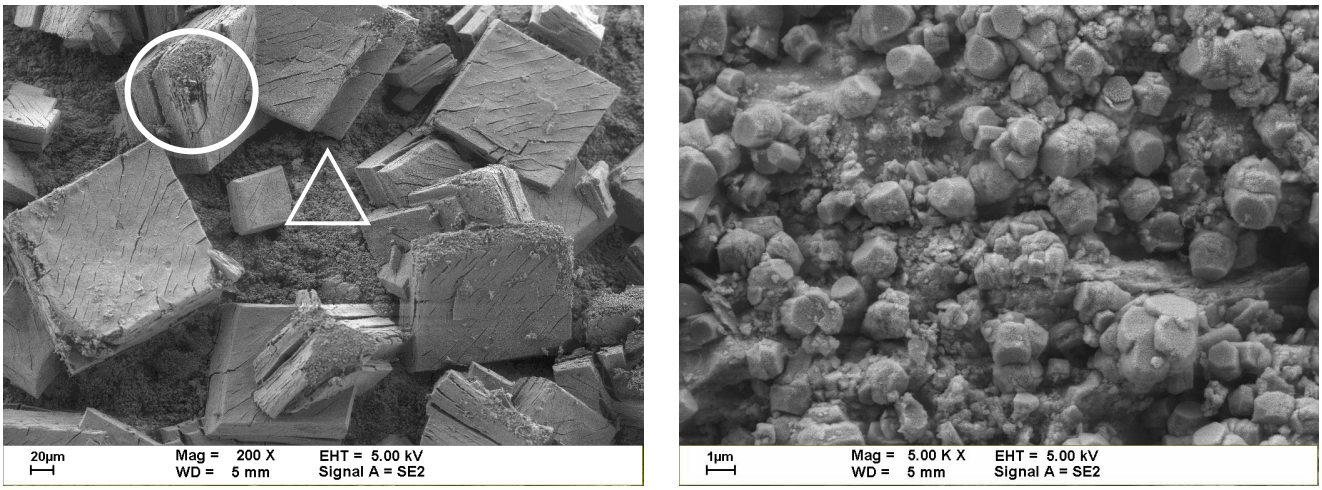

(**a**) (**b**)

The BET surface areas S_{BET} and other particle properties of Al_2O_3 support and MoS_2/γ-Al_2O_3 catalyst are listed in Table 1.

Table 1. The properties of γ-Al_2O_3 support and MoS_2/γ-Al_2O_3 catalyst.

Sample	S_{BET} (m^2 g^{-1})	Density (g cm^{-3})		Porosity	Pore size
		ρ_P	ρ_S	ε_P	(Å)
γ-Al_2O_3	280.46	1.27	2.89	0.528	55.5
MoS_2/γ-Al_2O_3	210.35	1.23	3.21	0.550	74.7

BET: Brunauer-Emmett-Teller; ρ_P: particle density; ρ_S: solid density.

It can be seen that the BET surface areas of Al_2O_3 and MoS_2/γ-Al_2O_3 prepared with concentration of ammonium heptamolybdate solution (C_{Mo}) = 10 wt.% are 280.5 and 210.4 m^2 g^{-1}, respectively. The average pore size of 55.5 Å of Al_2O_3 is smaller than that of 74.7 Å of MoS_2/γ-Al_2O_3. Thus the doping of MoS_2 enlarges the pore during preparation of catalyst, however, which in turn reduces the S_{BET}. Further accordingly, the porosity (ε_P) increases to 0.550 while bulk particle density ρ_P decreases to 1.23 g cm^{-3} for MoS_2/γ-Al_2O_3 after doping of MoS_2. The increase of true density or solid density ρ_S to 3.21 g cm^{-3} is due to the addition of MoS_2.on γ-Al_2O_3. The particle size of MoS_2/γ-Al_2O_3 is about 4–5 mm with average diameter of 4.09 mm which is only slightly larger than that of γ-Al_2O_3.of about 4 mm.

In the above, the XRD and SEM results confirm that the MoS_2 was successfully adopted on the Al_2O_3 support, ensuring the possession of activity by the MoS_2 which promotes the restructuring of CO via hydrogenation. The S_{BET} results of the catalyst indicate that a large portion of internal surface was retained, providing essential active sites for the adsorption and reactions.

3.2. Effect of Temperature T on the Catalytic Performance of MoS_2/γ-Al_2O_3

Table 2 illustrates the CO hydrogenation performances over MoS_2/γ-Al_2O_3 catalysts at various temperatures (from 423 to 573 K). It can be seen that the conversion of CO (X_{CO}) increases monotonously with the increasing temperature. At 573 K, the highest X_{CO} and the specific production rate (SPR) of hydrocarbons (HCs) are 8.2% and 16.1 mg h^{-1} g_{cat}^{-1}, respectively. However, a comparison of the yields of alkanes (Y_{Alk}) and alcohols (Y_{AOH}) shows that Y_{Alk} is greatly higher than Y_{AOH} at 573 K. Thus, when using MoS_2/γ-Al_2O_3 as the catalyst for the hydrogenation of CO, it is better to control the temperature around 523 K in order to harvest more AOH products.

The influences of temperature on the selectivities of HC products (S_{HC}) and specific production rates SPR of HCs over MoS_2/γ-Al_2O_3 catalysts are shown in Figure 4. The selectivities of ethanol (S_{EtOH}) exhibits the highest proportion of whole distribution at each T of 423, 473 and 523 K. However, at T = 573, S_{EtOH} decreases while that of methane (S_{CH4}) increases over S_{EtOH}. Note that C_2^+ alkanes denote C_2-C_4 alkanes, for which the selectivities (S_{C2+Alk}) also increase as the temperature increases. The increase of T not only changes the selectivities, but also enhances the conversion. In order to assess the roles of temperature and conversion on the selectivities, comparison of the results at T = 523 K and 573 K is made. These two different temperatures result in about the same conversions of 8.1–8.2, indicating that the changes of selectivities are mainly associated with higher temperature.

Figure 4. Selectivities (S) of hydrocarbon products (S_{HC}) and specific production rates (SPR) of HCs using MoS_2/γ-Al_2O_3 catalyst at various temperatures.

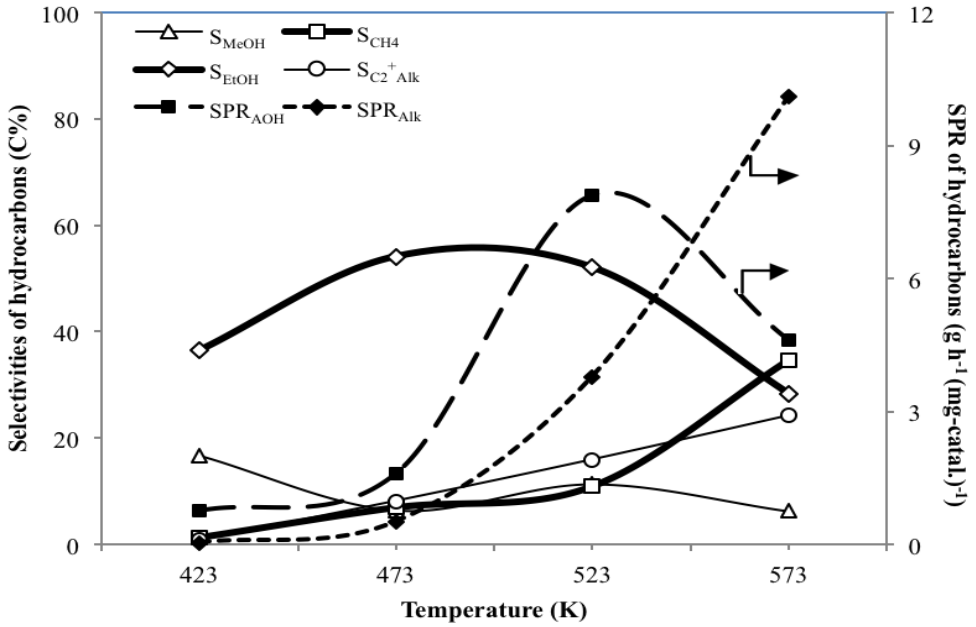

Table 2. Performance of hydrogenation of CO over $MoS_2/\gamma\text{-}Al_2O_3$ catalyst at various temperatures[a].

Catalyst	T (K)	Conversion of CO (X_{CO}) (C%)	SPR[b] (mg h^{-1} g_{cat}^{-1})		Yield[c] (C%)		Selectivity of hydrocarbon product[d] (C%) (S_{HC})							SPR_{HCs}[f]
			SPR_{Alk}	SPR_{AOH}	Y_{Alk}	Y_{AOH}	S_{CH4}	S_{C2+Alk}	S_{MeOH}	S_{EtOH}	S_{PrOH}	S_{BuOH}	S_{OtHC}[e]	(mg h^{-1} g_{cat}^{-1})
$MoS_2/\gamma\text{-}Al_2O_3$	423	0.6	0.1	0.8	0.2	0.5	1.2	0.7	16.7	36.4	6.5	7.3	31.1	1.1
	473	2.1	0.5	1.6	1.0	1.1	6.9	8.1	6.4	54.0	0.3	1.9	22.5	3.2
	523	8.1	3.8	7.9	2.0	5.0	10.9	15.8	11.3	52.0	2.3	0.3	7.5	13.2
	573	8.2	10.1	4.6	5.3	2.9	34.6	24.1	6.2	28.3	0.4	0.2	6.3	16.1
Rh-Mn/SiO_2[g]	563	3.6	46.1	205.8	-	-	-	-	-	56.8	-	-	-	-
	573	4.8	53.4	260.7	-	-	-	-	-	67.0	-	-	-	-
	583	7.4	127.6	314	-	-	-	-	-	49.5	-	-	-	-
	593	9.5	189	427	-	-	-	-	-	44.9	-	-	-	-

[a] Reaction conditions: P_{ST} = 30.6 atm (450 psi) (reading at 298 K), H_2/CO = 2, Q_G = 300 cm^3 min^{-1}, molar flow rate of CO = 0.2678 mole h^{-1}, GHSV = 1020 h^{-1}, m_S = 25 g; [b] SPR: Specific production rate; SPR_{Alk}, SPR_{AOH}: SPR of Alk, AOH; Alk: C_1 to C_4 alkanes; AOH: C_1 to C_4 alcohols; [c] $Y_j = (N_j M_j)/M_{CO,f}$, where N_j: number of carbon atoms in carbon-containing product j, M_j: mole of carbon-containing product j other than CO, $M_{CO,f}$: mole of carbon monoxide in feed. Y_{Alk} = sum of $Y_{cj\text{-}Alk}$, j = 1–4; Y_{AOH} = sum of $Y_{cj\text{-}AOH}$, j = 1–4; [d] $S_j = (N_j M_j)/(\Sigma N_j M_j)$; HC: Hydrocarbon; MeOH: methanol; EtOH: ethanol; PrOH: propanol; BuOH: butanol; C_2^+ Alk: ethane, propane, butane and pentane; [e.] OtHC: HCs other than C_1-C_4 alkanes and C_1-C_4 alcohols expressed equivalent to CH_4; [f] SPR of HCs: including C_1-C_4 alkanes, C_1-C_4 alcohols and OtHC; [g] P_{ST} = 29.6 atm (3.0 Mpa), H_2/CO = 2, SV = 27,000 mL g^{-1} h^{-1}, m_S = 0.3 g (~0.6 mL), Rh/Mn = 1 [26].

The comparison between SPR_{Alk} and SPR_{AOH}, shows that higher temperatures are favorable for the formation of alkanes, especially for CH_4. Further, a unique peak value of SPR_{AOH} of 7.9 mg h^{-1} g_{cat}^{-1} appears at T = 523 K that may indicate the optimal reaction temperature for higher AOH products rich in EtOH. Moreover, at T = 523 K, the higher production of alcohol products also restrains the amount of alkanes formed.

In a previous study concerning the effect of various temperatures over Rh-Mn/SiO_2 catalyst [26], the results indicated that the increasing temperature improves the X_{CO}, SPR_{Alk}, and SPR_{AOH}. Besides, there is also a peak value of S_{EtOH} at T = 573 K which is also a selectable temperature for producing EtOH as the target compound. The performance of MoS_2/γ-Al_2O_3 catalyst of this study is not as good as that of Rh-Mn/SiO_2 catalyst. However, the former catalyst is much cheaper than the latter one. The maximum S_{EtOH} of this study is 54% compared to 67% of Luo *et al.* [26], 4.8% of Egbebi and Spivey [23], 56.1% of Hu *et al.* [21] and 35.7% of Haider *et al.* [27].

3.3. Effect of H_2/CO Ratio $M_{H/C}$ on the Catalytic Performance

Although the ratio of H_2 and CO from biomass gasification is no more than 2, however, excess H_2 may be added for the adjustment of CO to produce more valuable products if feasible. Thus, the characteristics of production at 523 K using MoS_2/γ-Al_2O_3 catalysts with different $M_{H/C}$ are presented in Table 3. It shows a slight increase of X_{CO} from 7.6 to 8.3% as the $M_{H/C}$ increases from 1 to 4. However, for the consideration of the relative proportion of AOH to Alk products, the $M_{H/C}$ of 2 gives higher ratios of SPR_{AOH}/SPR_{Alk} and Y_{AOH}/Y_{Alk} than other $M_{H/C}$. This is consistent with the stoichiometric mole ratio of H_2 to CO of the synthesis reaction $2CO + 4H_2 \rightarrow C_2H_5OH + H_2O$, favoring the formation of ethanol.

As for the selectivities of HC products at various $M_{H/C}$, Figure 5 indicates that sum of selectivities of total AOH products are obviously higher than that of total alkane products, for which S_{EtOH} is dominant. The results illustrate that MoS_2/γ-Al_2O_3 is an alcohol favorite catalyst, particularly for EtOH. The favor of formation of AOH holds for other $M_{H/C}$ values of 1, 3 and 4 examined. Note that there is an increase of $C_2^+{}_{Alk}$ at $M_{H/C}$ = 1 due to the lack of H_2 for promoting the formation of other HCs. Thus, $M_{H/C}$ of 2 is proper for alcohol synthesis because of its high S_{AOH}, S_{EtOH} and SPR_{AOH}.

In a previous study as listed in Table 3, Egbebi and Spivey [23] showed a higher $M_{H/C}$ at 3 gives a higher S_{CH4} while a lower S_{EtOH} using alkane favorite catalyst of Rh-Mn-Li/TiO_2, which favors the reaction of $CO + 3H_2 \rightarrow CH_4 + H_2O$. Although the MoS_2/γ-Al_2O_3 catalyst employed in the present study does not favor the formation of CH_4 but ethanol, an increase of $M_{H/C}$ indeed slightly enhances its formation, consisting with the trend reported by Egbebi and Spivey [23].

Table 3. Performances of hydrogenation of CO over MoS_2/γ-Al_2O_3 catalysts at various H_2/CO[a].

Catalyst	H_2/CO (vol./vol.)	X_{CO} (C%)	SPR[b] ($mg\ h^{-1}\ g_{cat}^{-1}$)		Yield[c] (C%)		S_{HC}[d] (C%)							SPR_{HCs}[f]
			SPR_{Alk}	SPR_{AOH}	Y_{Alk}	Y_{AOH}	S_{CH4}	S_{C2+Alk}	S_{MeOH}	S_{EtOH}	S_{PrOH}	S_{BuOH}	S_{OtHC}[e]	($mg\ h^{-1}\ g_{cat}^{-1}$)
MoS_2/γ-Al_2O_3	1	7.6	4.6	6.4	2.7	4.1	11.8	26.2	9.0	44.9	1.8	1.2	5.1	11.9
	2	8.1	3.8	7.9	2.0	5.0	10.9	15.8	11.3	52.0	2.3	0.3	7.5	13.2
	3	8.0	4.1	7.8	2.2	4.8	12.7	16.3	12.7	48.7	2.1	0.5	7.0	13.3
	4	8.3	4.8	7.7	2.5	4.9	14.7	16.7	13.9	45.6	2.1	0.5	6.5	13.8
Rh-Mn-Li/TiO_2[g]	1	0.46	-	-	0.34	0.03	73.6	-	3.3	3.5	-	-	18.5	-
	2	0.94	-	-	0.74	0.07	78.4	-	3.4	4.3	-	-	13.0	-
	3	1.57	-	-	1.27	0.13	80.8	-	3.4	4.8	-	-	10.3	-

[a.] Reaction conditions: T = 523 K; other conditions are as specified in Table 2; [b–f.] As specified in Table 2; [g.] T = 543 K, P_{ST} = 19.7 atm (20 bar), Q_G = 220 mL min^{-1}, Rh/Mn/Li = 1/0.1/0.55 [23].

Figure 5. S_{AOH}, S_{Alk} and X_{CO} using MoS_2/γ-Al_2O_3 catalyst at different H_2/CO ratios (vol./vol.) at T = 523 K.

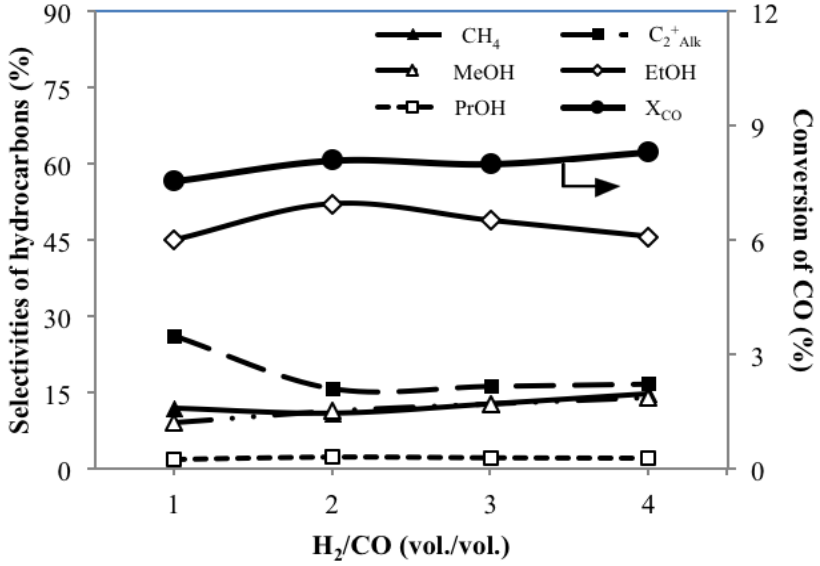

3.4. Effect of Total Gas Flow Rates Q_G on the Catalytic Performance

Table 4 illustrates the CO hydrogenation performances under the conditions of T = 523 K and $H_2/CO = 2$ with various Q_G over $MoS_2/\gamma\text{-}Al_2O_3$ catalysts. The X_{CO} significantly reduces from 8.1 to 4.1% as Q_G increases from 300 to 900 mL min^{-1} because of the decrease in reaction time (or gaseous retention time, t_R) with increasing Q_G. For the same reason, the Y_{Alk} and Y_{AOH} also exhibit decreasing trends with increasing Q_G. However, the SPRs of alcohol and HCs show rising trends from 7.9 to 18.0 mg h^{-1} g_{cat}^{-1} and 13.2 to 30.0 mg h^{-1} g_{cat}^{-1}, respectively, as Q_G increases. This is because more reactants are supplied with higher Q_G. For efficient utilization of reactants aiming at synthesizing AOH with higher X_{CO} and Y_{AOH}, a lower Q_G may meet the needs, but this is accompanied by a reduction in reactor productivity. The above said trend is also consistent with the findings of Hu *et al.* [21] concerning the effect of various GHSV and indicating that a lower GHSV improves the X_{CO} over $Rh\text{-}Mn/SiO_2$ catalyst.

Figure 6 further compares the S_{AOH}, S_{Alk} and X_{CO} at various Q_G for the case using $MoS_2/\gamma\text{-}Al_2O_3$ catalyst. It indicates the domination of S_{EtOH} over others. Moreover, the effect of Q_G on X_{CO} is more vigorous than on S_{AOH} and S_{Alk}. Combined evaluation of the role of Q_G on X_{CO} as well as the aforementioned Y_{AOH} suggests the use of lower Q_G.

Noting that the volume of catalysts divided by Q_G is equal to the 1/GHSV which represents the reaction time, the variation of X_{CO} with 1/GHSV was examined for elucidating the global reaction kinetics. Kinetics in the form of $d[CO]/dt = -k_n [CO]^n$ were then tested for the reaction order n = 0, 1 and 2 with the following linear equations:

$$1 - X_{CO} = 1 - (k_0/[CO]_0)\, t \text{ for } n = 0, \quad (10)$$

$$-\ln(1 - X_{CO}) = k_1\, t \text{ for } n = 1 \quad (11)$$

$$1/(1 - X_{CO}) = 1 + k_2\, [CO]_0\, t \text{ for } n = 2 \quad (12)$$

The correlation coefficients r^2 are 0.938, 0.945 and 0.951, respectively, for n = 0, 1 and 2. The fittings are re-plotted as $1 - X_{CO}$ *vs.* 1/GHSV as shown in Figure 7. The data for short 1/GHSV, say 3.5 s, are essentially linear and well fitted by the said three kinetic models as illustrated in Figure 7a, revealing negligible differences. However, the aforementioned three models exhibit differences which increase with increasing reaction time as indicated in Figure 7b. Further study on the mass transfer effect and the mechanism of the hydrogenation of CO, which may involve rather complicated reactions, on the reaction system would be helpful for establishing and confirming the proper kinetic model.

Table 4. Performances of hydrogenation of CO over $MoS_2/\gamma\text{-}Al_2O_3$ catalysts at various gas flow rates[a].

Catalyst	Q_G (mL min^{-1})	GHSV (h^{-1})	WHSV (h^{-1})	X_{CO} (C%)	SPR[b] (mg h^{-1} g$_{cat}^{-1}$)		Yield[c] (C%)		S_{HC}[d](C%)							SPR_{HCs}[f] (mg h^{-1} g$_{cat}^{-1}$)
					SPR_{Alk}	SPR_{AOH}	Y_{Alk}	Y_{AOH}	S_{CH4}	S_{C2+Alk}	S_{MeOH}	S_{EtOH}	S_{PrOH}	S_{BuOH}	S_{OtHC}[e]	
$MoS_2/\gamma\text{-}Al_2O_3$	300	1,020	0.34	8.1	3.8	7.9	2.0	5.0	10.9	15.8	11.3	52.0	2.3	0.3	7.5	13.2
	450	1,525	0.51	5.4	5.6	12.0	1.4	2.9	10.5	15.5	10.9	52.9	2.4	0.3	7.6	20.0
	600	2,035	0.69	4.8	6.4	14.3	1.2	2.6	10.4	14.9	11.2	51.1	2.3	0.3	7.8	23.6
	900	3,050	1.03	4.1	8.1	18.0	0.5	2.2	10.3	14.8	11.4	52.5	2.4	0.3	8.4	30.0
Rh-Mn/SiO_2[g]		1,700		38.7	-	-	15.6	21.9	40.2	-	2.8	53.9	-	-	3.1	-
		3,750		24.6	-	-	9.45	14.8	38.4	-	3.9	56.1	-	-	1.6	-

[a.] Reaction conditions: T = 523 K; other conditions are as specified in Table 2; [b–f.] As specified in Table 2; [g.] T= 573 K, P_{ST} = 53.3 atm (5.4 Mpa), H_2/CO = 2, m_S = 0.2 g, Rh/Mn = 4 [21].

Figure 6. S_{AOH}, S_{Alk} and X_{CO} using $MoS_2/\gamma\text{-}Al_2O_3$ catalyst at different total gas flow rates (Q_G) at T = 523 K.

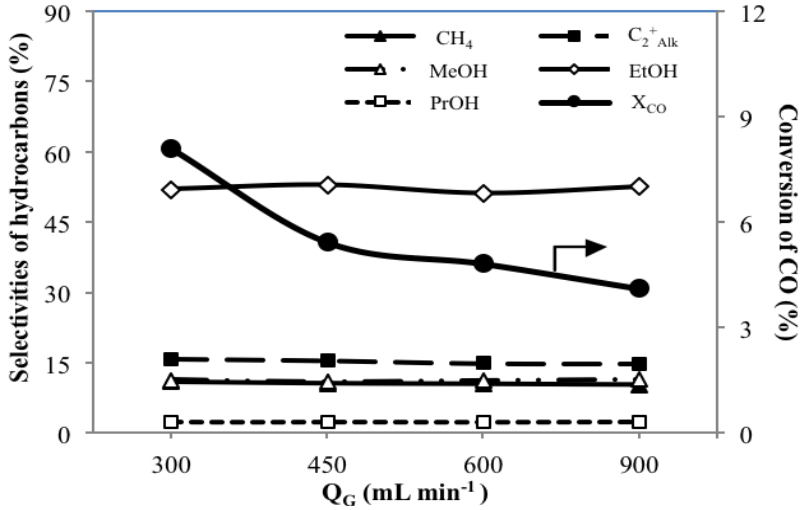

Figure 7. Plots of $1 - X_{CO}$ *vs.* 1/GHSV. (**a,b**): For short and long 1/GHSV. ○, □, Δ: Experimental data fitted by zero- (Zero), first- (1st), second- (2nd) order reaction kinetic models.

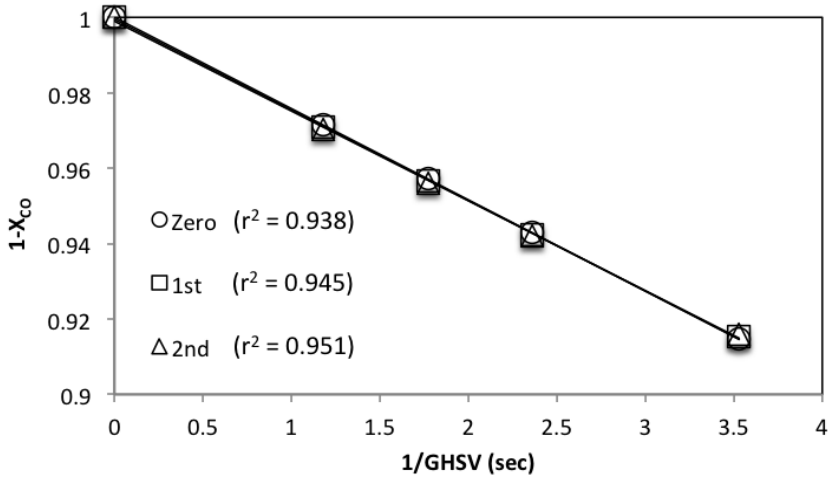

(**a**)

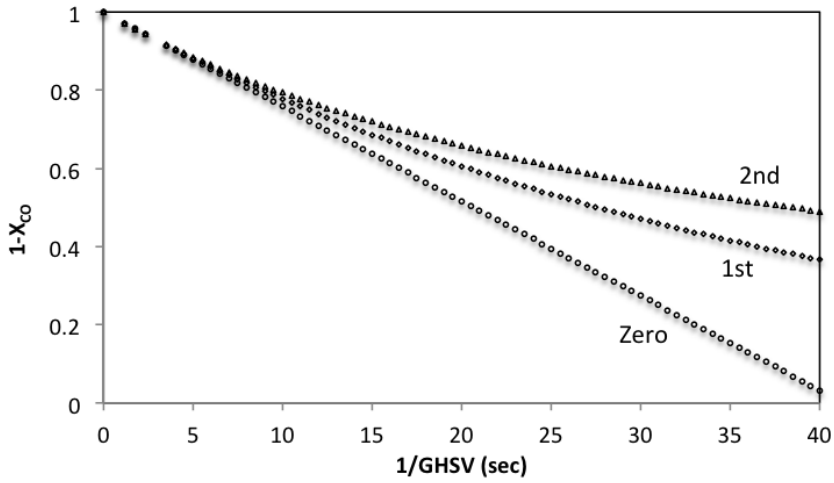

(**b**)

3.5. Effect of System Pressures P_{ST} on the Catalytic Performance

Table 5 illustrates the performances of hydrogenation of CO at various P_{ST} (from 255 to 540 psi) over MoS_2/γ-Al_2O_3 catalyst. It can be seen that X_{CO} increases monotonously with increasing pressure. At 540 psi, the highest X_{CO} and SPR_{HCs} are obtained, with values of 9.6% and 15.8 mg h^{-1} g_{cat}^{-1}, respectively. In addition, the SPR and Y also rise for alkanes as well as alcohol with increasing system pressure. A supply of higher pressure is equivalent to provide a larger amount of reactants into the reaction system, thus enhancing the reactions. Focusing on the SPR and Y of both Alk and AOH, it can be seen that an increasing pressure does not significantly change the relative proportions between the AOH and Alk, giving SPR_{AOH}/SPR_{Alk} of about 1.91–2.08 and Y_{AOH}/Y_{Alk} of about 2.18–2.52. Production of Alk as well as of AOH increases with pressure. Figure 8 shows the variations of S_{HCs} and X_{CO} with P_{ST}.

Table 5. Performances of hydrogenation of CO over MoS_2/γ-Al_2O_3 catalysts at various pressure[a].

Catalyst	P_{ST} (psi)	X_{CO} (C%)	SPR[b] (mg h^{-1} g_{cat}^{-1})		Yield[c] (C%)		S_{HC}[d](C%)							SPR_{HCs}[f] (mg h^{-1} g_{cat}^{-1})
			SPR_{Alk}	SPR_{AOH}	Y_{Alk}	Y_{AOH}	S_{CH4}	S_{C2+Alk}	S_{MeOH}	S_{EtOH}	S_{PrOH}	S_{BuOH}	S_{OtHC}[e]	
MoS_2/γ-Al_2O_3	225	4.6	2.2	4.2	1.2	2.7	10.3	18.3	9.9	50.9	2.5	-	8.1	7.4
	360	6.5	3.3	6.2	1.8	3.9	12.1	17.1	11.5	50.0	2.3	-	7.1	10.7
	450	8.1	3.8	7.9	2.0	5.0	10.9	15.8	11.3	52.0	2.3	0.3	7.5	13.2
	540	9.6	4.7	9.3	2.4	6.1	12.5	14.6	11.5	51.2	2.9	0.3	7.1	15.8
Fe/TiO_2[g]	206	6.7	-	-	-	-	36.2	7.2	3.3	35.7	-	-	17.6	-
	412	8.8	-	-	-	-	37.5	7.6	2.8	30.4	-	-	21.7	-

[a.] Reaction conditions: T = 523 K; other conditions are as specified in Table 2; [b–f.] As specified in Table 2; [g.] T = 543 K, H_2/CO = 1, Q_G = 20 mL min^{-1}, m_s = 2.65 g, weight hourly space velocity (WHSV) = 8,000 cm^3 h^{-1} g_{cat}^{-1} [27].

Figure 8. S_{AOH}, S_{Alk} and X_{CO} using MoS_2/γ-Al_2O_3 catalysts at different system pressures (P = P_{ST}) at T = 523 K.

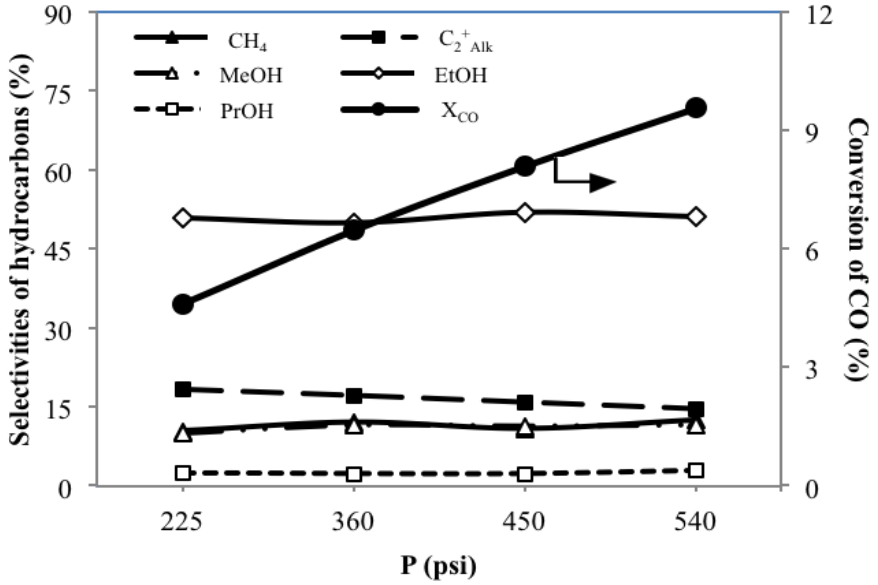

The results indicate that S_{EtOH} values of 50.9–52.0 C% are higher than the others. However, the variations of S_{HCs} of each HC with system pressure are minor. Thus, the main benefits of increasing P_{ST} are to enhance the aforesaid X_{CO}, Y_{Alk} and Y_{AOH}, reaching X_{CO} = 9.6%, Y_{Alk} = 2.4 C% and Y_{AOH} = 6.1 C% at 540 psi. In a previous study employing an alkane favoring Fe/TiO_2 catalyst, Haider *et al.* [27] also showed that an increasing pressure enhances the X_{CO} producing CH_4 with S_{CH4} as high as 37.5 C%.

Although the X_{CO} over $MoS_2/\gamma\text{-}Al_2O_3$ catalyst of 9.6% is only comparable to that of 9.5% using $Rh\text{-}Mn/SiO_2$ with Rh/Mn = 1 [26] while lower than that of 24.6%–38.7% employing $Rh\text{-}Mn/SiO_2$ with Rh/Mn = 4 [21], the $MoS_2/\gamma\text{-}Al_2O_3$ is more advantageous to use than the $Rh\text{-}Mn/SiO_2$ with Rh/Mn = 4 because it is relatively cheap and easy to make. However, for commercialization, the X_{CO} should be improved. Thus, modification of MoS_2 catalyst by some cheap ways to enhance its activity would be very desirable and useful. An increase of reaction time may also enhance the conversion.

4. Conclusions

1. For the hydrogenation of CO using $MoS_2/\gamma\text{-}Al_2O_3$ catalyst, T at 523 K is proper not only to yield SPR_{AOH} and Y_{AOH} higher than SPR_{Alk} and Y_{Alk}, respectively, but also to give a satisfactory high value of S_{EtOH} of 52.0 C%.
2. Compared to other settings of H_2/CO, H_2/CO at 2 gives highest S_{EtOH} of 52.0 C%, which is in accordance with the stoichiometry of the formation of EtOH.
3. A lower Q_G offers longer t_R, resulting in higher reaction extents with higher X_{CO} and Y_{AOH} along with a significantly high value of S_{EtOH} of 52.0 C%.
4. An increasing pressure enhances the X_{CO}, Y_{Alk} and Y_{AOH}, while only slightly changing the S_{HCs} of each HC.
5. The beneficial use of $MoS_2/\gamma\text{-}Al_2O_3$ in the hydrogenation of CO favors the production of ethanol with the proper operation conditions at T = 523 K, H_2/CO = 2, lower flow rate and higher pressure.

Acknowledgements

The authors gratefully acknowledge the National Science Council, Taiwan for supporting this study.

References

1. Spivey, J.J.; Egbebi, A. Heterogeneous catalytic synthesis of ethanol from biomass-derived syngas. *Chem. Soc. Rev.* **2007**, *36*, 1514–1528.
2. Subramani, V.; Gangwal, S.K. A review of recent literature to search for an efficient catalytic process for the conversion of syngas to ethanol. *Energy Fuels* **2008**, *22*, 814–839.
3. Mori, S. Development of utilization technologies of biomass energy. *J. Environ. Eng. Manag.* **2009**, *19*, 67–72.
4. Pambudi, N.A.; Torii, S.; Saptoadi, H.; Sumbodo, W.; Syamsiyo, M.; Surono, U.B. Experimental study on combustion of biobriquettes jatropha curcas solid waste. *J. Environ. Eng. Manag.* **2010**, *20*, 133–136.

5. Chuang, Y.S.; Chen, C.C.; Lay, C.H.; Sung, I.Y.; Wu, J.S.; Lee, S.C.; Sen, B.; Lin, C.Y. Optimization of incubation factors for fermentative hydrogen production from agricultural wastes. *Sustain. Environ. Res.* **2012**, *22*, 99–106.
6. Syu, F.S.; Chiueh, P.T. Process simulation of rice straw torrefaction. *Sustain. Environ. Res.* **2012**, *22*, 177–183.
7. Ragauskas, A.J.; Williams, C.K.; Davison, B.H.; Britovsek, G.; Cairney, J.; Eckert, C.A.; Frederick, W.J.; Hallett, J.P.; Leak, D.J.; Liotta, C.L.; Mielenz, J.R.; Murphy, R.; Templer, R.; Tschaplinski, T. The path forward for biofuels and biomaterials. *Science* **2006**, *311*, 484–489.
8. Burch, R.; Hayes, M.J. The preparation and characterisation of Fe-promoted Al_2O_3-supported Rh catalysts for the selective production of ethanol from syngas. *J. Catal.* **1997**, *165*, 249–261.
9. Mazzocchia, C.; Gronchi, P.; Kaddouri, A.; Tempesti, E.; Zanderighi, L.; Kiennemann, A. Hydrogenation of CO over Rh/SiO_2-CeO_2 catalysts: Kinetic evidences. *J. Mol. Catal. A Chem.* **2001**, *165*, 219–230.
10. Ojeda, M.; Granados, M.L.; Rojas, S.; Terreros, P.; Garcia-Garcia, F.J.; Fierro, J.L.G. Manganese-promoted Rh/Al_2O_3 for C-2-oxygenates synthesis from syngas—Effect of manganese loading. *Appl. Catal. A Gen.* **2004**, *261*, 47–55.
11. Koizumi, N.; Murai, K.; Ozaki, T.; Yamada, M. Development of sulfur tolerant catalysts for the synthesis of high quality transportation fuels. *Catal. Today* **2004**, *89*, 465–478.
12. Li, D.B.; Yang, C.; Qi, H.J.; Zhang, H.R.; Li, W.H.; Sun, Y.H.; Zhong, B. Higher alcohol synthesis over a La promoted $Ni/K_2CO_3/MoS_2$ catalyst. *Catal. Commun.* **2004**, *5*, 605–609.
13. Li, D.B.; Zhao, N.; Qi, H.J.; Li, W.H.; Sun, Y.H.; Zhong, B. Ultrasonic preparation of Ni modified K_2CO_3/MoS_2 catalyst for higher alcohols synthesis. *Catal. Commun.* **2005**, *6*, 674–678.
14. Li, D.; Yang, C.; Zhao, N.; Qi, H.; Li, W.; Sun, Y.; Zhong, B. The performances of higher alcohol synthesis over nickel modified K_2CO_3/MoS_2 catalyst. *Fuel Process. Technol.* **2007**, *88*, 125–127.
15. Woo, H.C.; Park, T.Y.; Kim, Y.G.; Nam, I.S.; Lee, J.S.; Chung, J.S. Alkali-promoted MoS_2 catalysts for alcohol synthesis—The effect of alkali promotion and preparation condition on activity and selectivity. *Stud. Surf. Sci. Catal.* **1993**, *75*, 2749–2752.
16. Sakashita, Y.; Araki, Y.; Shimada, H. Effects of surface orientation of alumina supports on the catalytic functionality of molybdenum sulfide catalysts. *Appl. Catal. A Gen.* **2001**, *215*, 101–110.
17. Qi, H.J.; Li, D.B.; Yang, C.; Ma, Y.G.; Li, W.H.; Sun, Y.H.; Zhong, B. Nickel and manganese co-modified K/MoS_2 catalyst: High performance for higher alcohols synthesis from CO hydrogenation. *Catal. Commun.* **2003**, *4*, 339–342.
18. Huang, M.; Cho, K. Density functional theory study of CO hydrogenation on a MoS_2 surface. *J. Phys. Chem. C* **2009**, *113*, 5238–5243.
19. Surisetty, V.R.; Dalai, A.K.; Kozinski, J. Effect of Rh promoter on MWCNT-supported alkali-modified MoS_2 catalysts for higher alcohols synthesis from CO hydrogenation. *Appl. Catal. A Gen.* **2010**, *381*, 282–288.
20. Inoue, T.; Iizuka, T.; Tanabe, K. Hydrogenation of carbon dioxide and carbon monoxide over supported rhodium catalysts under 10 bar pressure. *Appl. Catal.* **1989**, *46*, 1–9.
21. Hu, J.; Wang, Y.; Cao, C.; Elliott, D.C.; Stevens, D.J.; White, J.F. Conversion of biomass-derived syngas to alcohols and C_2 oxygenates using supported Rh catalysts in a microchannel reactor. *Catal. Today* **2007**, *120*, 90–95.

22. Mazzocchia, C.; Tempesti, E.; Gronchi, P.; Giuffrè, L.; Zanderighi, L. Hydrogenation of CO over ZrO_2-supported Rh catalysts: Role of experimental parameters in modifying the $C_2H_5OHCH_4$ product ratio. *J. Catal.* **1988**, *111*, 345–352.
23. Egbebi, A.; Spivey, J.J. Effect of H_2/CO ratio and temperature on methane selectivity in the synthesis of ethanol on Rh-based catalysts. *Catal. Commun.* **2008**, *9*, 2308–2311.
24. Berdinsky, A.S.; Chadderton, L.T.; Yoo, J.B.; Gutakovsky, A.K.; Fedorov, V.E.; Mazalov, L.N.; Fink, D. Structural changes of MoS_2 nano-powder in dependence on the annealing temperature. *Appl. Phys. A Mater. Sci. Process.* **2005**, 80, 61–67.
25. Ye, L.; Wu, C.; Guo, W.; Xie, Y. MoS_2 hierarchical hollow cubic cages assembled by bilayers: One-step synthesis and their electrochemical hydrogen storage properties. *Chem. Commun.* **2006**, *45*, 4738–4740.
26. Luo, H.Y.; Lin, P.Z.; Xie, S.B.; Zhou, H.W.; Xu, C.H.; Huang, S.Y.; Lin, L.W.; Liang, D.B.; Yin, P.L.; Xin, Q. The role of Mn and Li promoters in supported rhodium catalysts in the formation of acetic acid and acetaldehyde. *J. Mol. Catal. A Chem.* **1997**, *122*, 115–123.
27. Haider, M.A.; Gogate, M.R.; Davis, R.J. Fe-promotion of supported Rh catalysts for direct conversion of syngas to ethanol. *J. Catal.* **2009**, *261*, 9–16.